

Observation and theory of reorientation-induced spectral diffusion in polarization-selective 2D IR spectroscopy

Patrick L. Kramer,^{a)} Jun Nishida,^{a)} Chiara H. Giammanco, Amr Tamimi, and Michael D. Fayer^{b)}

Department of Chemistry, Stanford University, Stanford, California 94305, USA

(Received 23 March 2015; accepted 29 April 2015; published online 14 May 2015)

In nearly all applications of ultrafast multidimensional infrared spectroscopy, the spectral degrees of freedom (e.g., transition frequency) and the orientation of the transition dipole are assumed to be decoupled. We present experimental results which confirm that frequency fluctuations can be caused by rotational motion and observed under appropriate conditions. A theory of the frequency-frequency correlation function (FFCF) observable under various polarization conditions is introduced, and model calculations are found to reproduce the qualitative trends in FFCF rates. The FFCF determined with polarization-selective two-dimensional infrared (2D IR) spectroscopy is a direct reporter of the frequency-rotational coupling. For the solute methanol in a room temperature ionic liquid, the FFCF of the hydroxyl (O–D) stretch decays due to spectral diffusion with different rates depending on the polarization of the excitation pulses. The 2D IR vibrational echo pulse sequence consists of three excitation pulses that generate the vibrational echo, a fourth pulse. A faster FFCF decay is observed when the first two excitation pulses are polarized perpendicular to the third pulse and the echo, $\langle XXYY \rangle$, than in the standard all parallel configuration, $\langle XXXX \rangle$, in which all four pulses have the same polarization. The 2D IR experiment with polarizations $\langle XYXY \rangle$ (“polarization grating” configuration) gives a FFCF that decays even more slowly than in the $\langle XXXX \rangle$ configuration. Polarization-selective 2D IR spectra of bulk water do not exhibit polarization-dependent FFCF decays; spectral diffusion is effectively decoupled from reorientation in the water system. © 2015 AIP Publishing LLC. [<http://dx.doi.org/10.1063/1.4920949>]

I. INTRODUCTION

Polarization control of the incident beams and emitted signals has proven to be a powerful and useful feature in nonlinear optical spectroscopy. Separation of pump-probe (PP) signals into the isotropic signal (population) and anisotropy (orientational correlation function) decays is a very common example.^{1–4} In two-dimensional infrared (2D IR) vibrational echo spectroscopy, each of the four field interactions can be manipulated separately, giving even more freedom in utilizing polarization control. Such polarization-selective 2D IR experiments are frequently leveraged to determine the angles between coupled transition dipoles,^{5–7} measure jump angles during chemical exchange events,⁸ suppress diagonal peaks in favor of cross peaks,^{9,10} and select desired signals from unwanted background such as scatter¹¹ or excitation beams.¹²

Whether explicit or not, nearly all of these applications assume that the spectral dynamics (frequency fluctuations) are independent of the orientational motions of the vibrational transition dipole under study. Formally, the assumption is that the third order nonlinear response function factors into orientational and vibronic contributions,^{3,4,13,14}

$$R_{\eta\gamma\beta\alpha}^{(3)}(t_1, t_2, t_3) = R_{\eta\gamma\beta\alpha}(t_1, t_2, t_3)R_V(t_1, t_2, t_3). \quad (1)$$

The first factor in (1), a tensor, carries all the polarization dependence (η, \dots, α) and accounts for the independent reorientation dynamics¹³ during each of the intervals t_1, \dots, t_3 (delays between successive electric field/dipole interactions). $R_{\eta\gamma\beta\alpha}$ also encodes spatial parameters, such as relative transition dipole directions.⁶ The R_V factor is isotropic and contains all spectral degrees of freedom such as the pure dephasing and spectral diffusion dynamics of the vibrational modes. Often, the factorization in (1) may be justified by a separation of timescales between the probe reorientation and the structural fluctuations which cause the vibronic response to evolve.^{13,14}

The 2D IR techniques are used extensively for the decomposition of inhomogeneously broadened vibrational bands in condensed phases, through time dependent 2D IR line shape analysis, into the timescales and amplitudes of the various dynamical processes that contribute to the broadening.^{15–20} The structural dynamics produce frequency evolution that samples the inhomogeneously broadened absorption line. These dynamics are quantified by the frequency-frequency correlation function (FFCF), which completely determines the 2D IR line shape under most conditions.^{4,5} The FFCF can be extracted from experimental 2D IR spectra with techniques such as the center line slope (CLS) method.^{16,17} The polarization dependence of 2D IR vibrational line shapes has previously not been explored in depth. The 2D IR anisotropy spectrum of water has been examined to observe hydroxyl reorientation accompanying hydrogen bond switching,^{8,21,22} but the potential role of reorientation of the vibrational

^{a)}P. L. Kramer and J. Nishida contributed equally to this work.

^{b)}Author to whom correspondence should be addressed. Electronic mail: fayer@stanford.edu

transition dipole in determining the 2D IR line shape itself has not been discussed.

If approximation (1) holds, the nonlinear signal observed with different polarization configurations will have different initial amplitudes and amplitude decay rates due to the field polarization and transition dipole reorientation,¹³ but the same normalized 2D line shape will be obtained with any polarization configuration. However, there is a clear case in which Eq. (1) does not hold. Suppose a vibrational probe is introduced into a relatively slowly evolving environment, e.g., the global structure in a room temperature ionic liquid (RTIL), such that the probe itself can reorient on a much faster timescale than the complete structural evolution of the environment. If the interaction with the vibration, which at least in part determines its frequency, is a vector, e.g., an electric field through the Stark effect, then the angular coordinates of the vibrational probe relative to the external environment can contribute to its instantaneous frequency. Reorientation is then a source of spectral diffusion,²³ i.e., the evolution of a molecule's absorption frequency over time, which causes the FFCF to decay. In the presence of this reorientation-induced spectral diffusion (RISD),²³ the separation of angular and spectral coordinates no longer holds, and hence the time dependent 2D IR line shape will in general depend on the polarizations of the excitation beams (α, β, γ) and emitted signal (η). The breakdown of Eq. (1) has been previously indicated by the observation of variations in a one-dimensional pump-probe spectrum with different pump polarizations.²⁴ The variation was attributed to vibrational probe reorientation occurring rapidly on the timescale of vibrational dephasing, resulting in a non-factorizing total third order response.²⁴ However, to our knowledge, the RISD process has not been directly observed in time domain previously. Here, we report observation of such spectral diffusion induced by reorientation of a vibrational probe by polarization-selective 2D IR spectroscopy of dilute methanol in a room temperature ionic liquid.

II. EXPERIMENTAL METHODS

The experimental techniques for polarization-selective IR PP and 2D IR vibrational echo experiments have been described in detail previously.^{15,25} Briefly, for polarization-selective 2D IR experiments, three excitation pulses with variable delays cross in the sample in the box-CARS geometry, and the vibrational echo signal is emitted in the phase matched direction. The signal is overlapped spatially and temporally with the local oscillator (LO) pulse, which is attenuated and fixed at horizontal polarization by a pair of polarizers. The heterodyned signal is frequency dispersed with a monochromator (configured as a spectrograph) and detected with a 32-element liquid nitrogen cooled mercury cadmium telluride (MCT) array. No additional polarization optics are added to achieve the $\langle XXXX \rangle$ polarization configuration. For the $\langle XYY \rangle$ and $\langle XYXY \rangle$ configurations, half wave plates and polarizers (nanoparticle linear film, Thorlabs) are used to set two of the excitation beams at vertical polarization. Beams 1 and 2 are vertically polarized for $\langle XYY \rangle$, while beams 1 and 3 are set vertical for $\langle XYXY \rangle$.

The time delay between pulses 1 and 2 is τ (or t_1 in Eq. (1)) and that between 2 and 3 is T_w (or t_2). A fourth pulse, the LO, is made time-coincident with pulse 3 (and the signal pulse, at $\tau = 0$). Pulse 1 labels the initial oscillation frequency of a transition, and the system is in a coherence state over the period τ . Pulse 2 ends the first coherence period and begins the waiting time, T_w , during which the system propagates its dynamics in a population state. Finally, pulse 3 begins a second coherence period, t (or t_3), during which the third order signal is radiated and heterodyned with the local oscillator, providing phase resolution and amplifying the weak signal. The oscillator frequency of a particular molecule during τ and t need not be the same. Fourier transformations of the nonlinear signal are performed over the two coherence periods. The one over t is done by the spectrograph, which takes the echo/LO wave packet into the frequency domain. This Fourier transform gives the vertical axis in the 2D spectrum, ω_m . The Fourier transform over τ , which is scanned at each T_w to produce a temporal interferogram at each ω_m , is done numerically. This Fourier transform gives the horizontal axis in the 2D spectrum, ω_τ . The resulting 2D spectrum correlates initial oscillation frequencies ω_τ with their final frequencies ω_m .

The dynamical information, i.e., the FFCF, is encoded in the change of the 2D line shape with waiting time, T_w . The FFCF is extracted from these 2D line shape changes via the CLS technique.^{16,17} The CLS is typically fit to a sum of exponentials. While it will be shown in Sec. IV that the polarization resolved FFCF is not necessarily a sum of exponentials in the presence of RISD, this form still allows a convenient description of the data.

In the present work, we utilize the CLS- ω_m method, which has been shown to be mathematically equivalent to the T_w -dependent part of the normalized FFCF.¹⁷ With the CLS method, the experimental center line slope data and linear absorption spectrum (Figure S1 in supplementary material)²⁶ can be used to obtain the complete FFCF, which has the form

$$C(t) = \langle \delta\omega(t)\delta\omega(0) \rangle = \frac{\delta(t)}{T_2} + \sum_i \Delta_i^2 \exp(-t/\tau_i). \quad (2)$$

Here, $\delta\omega(t) = \omega(t) - \langle \omega \rangle$ is the instantaneous frequency fluctuation, $T_2 = 1/(\pi\Gamma)$ is the total homogeneous dephasing time (with Γ the homogeneous linewidth), Δ_i is the frequency fluctuation amplitude of the i th inhomogeneous contribution to the line shape, and τ_i is the correlation time of component i (equal to the i th exponential time constant from the CLS decay). The ensemble average $\langle \dots \rangle$ refers to whichever ensemble corresponds to the experimental conditions (i.e., polarization configuration).

The homogeneous term arises from a motionally narrowed contribution to the FFCF that occurs if one of the components of the frequency fluctuations meets the condition $\Delta_i\tau_i \ll 1$. In this case, Δ_i and τ_i cannot be determined separately and a homogeneous component with pure dephasing linewidth $\Gamma^* = \Delta_i^2\tau_i = 1/(\pi T_2^*)$ results. The total homogeneous dephasing time is given by¹⁶

$$\frac{1}{T_2} = \frac{1}{T_2^*} + \frac{1}{2T_1} + \frac{1}{3T_{\text{or}}}, \quad (3)$$

where T_1 is the vibrational lifetime and T_{or} is the orientational correlation time. The CLS gives the correct τ_i and the relative Δ_i . The total homogeneous dephasing time T_2 and the values of the Δ_i in units of frequency are obtained from the experimental data from a simultaneous fit to the CLS decay and the experimental linear absorption line shape.^{4,16,17}

Further details regarding the laser system, 2D IR data processing, polarization-selective PP experiments, and sample preparation may be found in the supplementary material.²⁶

III. EXPERIMENTAL RESULTS

A series of polarization-selective 2D IR spectra were obtained on the O–D (deuterated hydroxyl) stretch of methanol- d_4 in the RTIL 1-hexyl-3-methylimidazolium hexafluorophosphate (HmimPF₆). The methanol solute was diluted to effective isolation^{27–29} (20 ion pairs per methanol). The experiments were conducted in an identical manner²⁵ for each of the three polarization configurations: $\langle XXXX \rangle$, $\langle XXYY \rangle$, and $\langle XYXY \rangle$ (note that $\langle XYXY \rangle$ equals $\langle XYYX \rangle$ for a single dipole transition^{13,30}). Spectra were taken at waiting times T_w (or t_2 , delay between the second and third field interactions) between 160 fs and 50 ps.

Representative 2D spectra of the 0-1 (ground to first excited state) region of the O–D stretch at $T_w = 20$ ps for each

polarization configuration are shown in Figure 1(a). These spectra correlate an initial vibrational oscillator frequency ω_τ on the horizontal axis with its final oscillator frequency ω_m on the vertical axis, observed after the waiting time, T_w . The solid blue lines are the center lines.¹⁷ A steeper CLS arises from greater correlation of the 2D line shape along the diagonal and therefore less extent of spectral diffusion. The $\langle XXXX \rangle$ and $\langle XXYY \rangle$ spectra appear similar, but are not identical. The CLS obtained for $\langle XYXY \rangle$ (polarization grating configuration), however, is considerably greater than that of the other two pathways. It is quite evident by inspection that the $\langle XYXY \rangle$ 2D line shape is less rounded than that in the parallel and perpendicular polarization spectra. Figure 1(b) shows the center lines reproduced from the three 2D spectra in Fig. 1(a) superimposed and expanded as an aid to the eye. The differences in the slopes are clear.

The full CLS decays for each polarization configuration appear in Figure 1(c) (points). Biexponential decay functions provide a convenient means of quantifying the differences between the CLS decays obtained with different polarization configurations; the fits are the solid curves. The components of these fits can be assigned to their respective spectral weights, providing the full FFCFs, using the CLS method^{16,17} (Sec. II). These FFCF parameters are given in Table I.

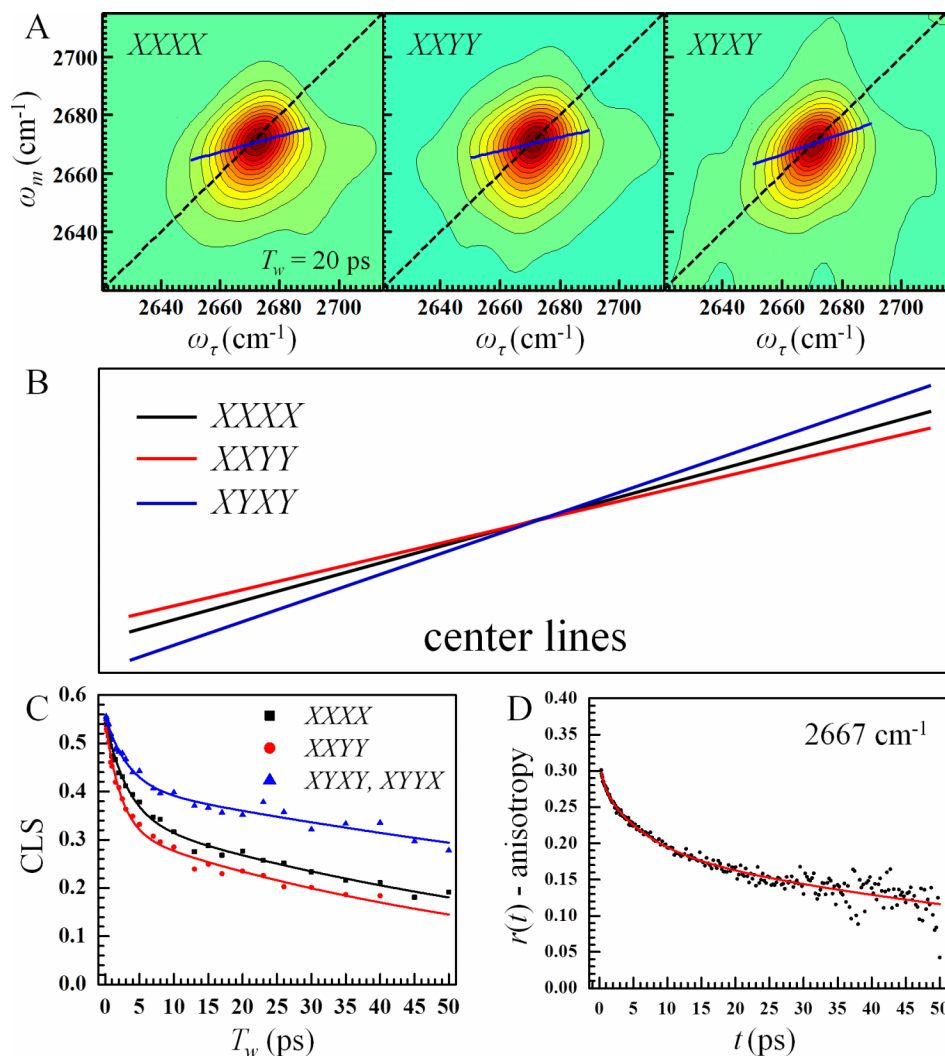


FIG. 1. Spectral diffusion and orientational relaxation results for methanol- d_4 in HmimPF₆. (a) 2D IR spectra in the 0-1 region at the same waiting time, $T_w = 20$ ps, with polarization configurations $\langle XXXX \rangle$, $\langle XXYY \rangle$, and $\langle XYXY \rangle$. Black dotted lines are the diagonals, and the solid blue lines are the fits to the center lines from which the CLS is determined. (b) The center lines from (a) superimposed so the difference in slopes can be visualized. The center lines have been extended as an aid to the eye. (c) CLS waiting time dependence for each polarization configuration (points). Solid curves are biexponential fits to the data. (d) The pump-probe anisotropy $r(t)$ (points) taken at detection frequency 2667 cm⁻¹, approximately the line center (see absorption spectrum in supplementary material, Fig. S1).²⁶ The red curve is a triexponential fit giving time constants 0.7 ± 0.6 ps, 7 ± 2 ps, and 96 ± 12 ps for the orientational relaxation. .

TABLE I. FFCF parameters for methanol-d₄ in HmimPF₆ with three polarization configurations.^a

Polarization	T_2 (ps)	Γ (cm ⁻¹)	Δ_1 (cm ⁻¹)	τ_1 (ps)	Δ_2 (cm ⁻¹)	τ_2 (ps)
$\langle XYYX \rangle$	1.07 ± 0.04	9.9 ± 0.4	4.4 ± 0.1	2.2 ± 0.4	5.2 ± 0.1	63 ± 6
$\langle XXXX \rangle$	1.11 ± 0.04	9.5 ± 0.3	4.2 ± 0.1	3.2 ± 0.4	5.5 ± 0.1	76 ± 7
$\langle YXYX \rangle$	1.14 ± 0.04	9.3 ± 0.3	3.5 ± 0.1	3.3 ± 0.6	5.9 ± 0.1	149 ± 19

^aThe complete FFCF is obtained from the experimental CLS data (Fig. 1(c)) and linear absorption spectrum (Fig. S1); see Sec. II and supplementary material.²⁶ T_2 is the total dephasing time, $\Gamma = 1/(\pi T_2)$ is the FWHM of the Lorentzian homogeneous linewidth, and the frequency fluctuation amplitudes Δ_1 and Δ_2 are standard deviations of the Gaussian inhomogeneous line shapes, which are convolved for the total inhomogeneous contribution ($\Delta_{\text{total}}^2 = \Delta_1^2 + \Delta_2^2$). All three tensor elements give a total inhomogeneous linewidth of ~ 16 cm⁻¹ (given as FWHM = 2.355 × Δ_{total}).

Several important features are apparent from Fig. 1(c) and Table I. All three decays begin from a CLS value of ~ 0.55 at $T_w = 160$ fs. The nearly instantaneous drop from a slope of 1 (complete correlation at zero waiting time) is caused by the homogeneous broadening.^{16,17} As reported in Table I, the homogeneous linewidths Γ are the same within experimental error for all three polarization configurations. The ultrafast (typically less than 100 fs) structural and orientational fluctuations, which cause homogeneous dephasing during coherence periods and result in a motionally narrowed contribution to the FFCF, are identical in each 2D IR polarization configuration. During the first 10 ps, the CLS decays with decay time constants on the order of 3 ps (see Table I) for each polarization configuration. However the perpendicular decay is somewhat faster than the other two; the difference in time constants is just outside the error bars. The data sets decay to different amplitudes on the ~ 3 ps timescale. While $\langle XYYX \rangle$ has reached a CLS of about 0.28 by $T_w = 10$ ps, $\langle XXXX \rangle$ gives 0.32 and $\langle YXYX \rangle$ still has a much larger CLS of 0.40. The fastest frequency fluctuation amplitude (following the homogeneous component), Δ_1 , reflects this ordering. It is largest for the perpendicular configuration and smallest for $\langle YXYX \rangle$. By the end of our accessible T_w range (limited by the O–D stretch vibrational lifetime), the parallel and perpendicular CLSs have reached a similar value of ~ 0.19 , while the $\langle YXYX \rangle$ CLS remains quite high at 0.28. The long-time spectral diffusion time constant for perpendicular is somewhat faster than for parallel, but the values are just within the error bars. The decay for $\langle YXYX \rangle$ is about twice as slow (see Table I).

Polarization-selective PP experiments were used to obtain the isotropic PP decay and the anisotropy $r(t)$ (see supplementary material).²⁶ The vibrational lifetime was determined from the isotropic PP signal.²⁸ The lifetime at the signal peak (2667 cm⁻¹) is 16.9 ± 0.1 ps. The anisotropy is proportional to $C_2(t)$, the second Legendre polynomial orientational correlation function of the transition dipole (parallel to the O–D bond vector^{29,31}). A value of $r = 0.4$ at time zero indicates complete orientational correlation. The orientational correlation decay has a similar form at all detected wavelengths; data for 2667 cm⁻¹ are shown in Figure 1(d). We can clearly identify three well-separated timescales on which orientational randomization occurs, beyond the inertial drop from 0.4 in the first ~ 100 fs.^{32,33} There is considerable reorientation on all time scales during which the CLS and FFCF decay due to spectral diffusion. It appears likely, therefore, that reorientation-induced spectral diffusion is a significant contributor to the CLS decay of methanol in this ionic liquid.

IV. THEORY

We can understand the influence of reorientation-induced spectral diffusion on the CLS observable first in an intuitive manner. Consider a vibration that has its frequency at least in part determined by its interaction with an electric field through the Stark effect,^{34,35} with a non-negligible electric field component which is static on the time scale of the orientational relaxation. The Stark coupling depends on $\delta\vec{\mu} \cdot \vec{E}$, where $\delta\vec{\mu}$ is the difference in dipole moment between the vibrational excited state and ground state, and \vec{E} is the electric field. Then as the molecule rotates, the $\delta\vec{\mu}$ direction (which is expected to be parallel to the transition dipole, see supplementary material²⁶) changes, which alters the vibrational frequency. In the parallel configuration, molecules will tend to be excited with the same polarization that gives rise to the signal. As they rotate, their frequencies will change, but they will also rotate into directions that contribute less to the signal. Therefore, the RISD will be somewhat mitigated by the reduction in the contribution of the reoriented molecules to the detected 2D IR signal. In the perpendicular configuration, molecules will be initially excited with their transition dipoles in directions that tend to be perpendicular to the signal polarization. As they rotate, their frequencies change and their transition dipoles will tend to move toward the readout polarization. Therefore, as rotation changes their frequency, they also contribute more to the 2D IR signal, amplifying their contribution to RISD. The result is that RISD in $\langle XYYX \rangle$ makes a greater contribution, resulting in faster spectral diffusion than in $\langle XXXX \rangle$. The $\langle YXYX \rangle$ configuration produces a signal for which reorientation removes molecules from observation even more readily than $\langle XXXX \rangle$.¹³ Thus, RISD in $\langle YXYX \rangle$ will contribute less to the spectral diffusion than in $\langle XXXX \rangle$. These qualitative considerations are consistent with the experimental observations presented in Sec. III.

We developed a procedure to quantify the difference in CLS decays between the parallel and perpendicular pumped ($\langle XXXX \rangle$ and $\langle XYYX \rangle$) ensembles. We introduce a dynamic quantity referred to as the polarization-weighted frequency-frequency correlation function (PW-FFCF). The standard FFCF is given by

$$\langle \delta\omega(t)\delta\omega(0) \rangle = \frac{1}{N} \sum_i \delta\omega_i(t)\delta\omega_i(0), \quad (4)$$

where $\delta\omega_i(t) = \omega_i(t) - \langle \omega \rangle$ is the instantaneous frequency fluctuation of molecule i , $\langle \dots \rangle$ denotes an ensemble average, and N is the number of the molecules. The PW-FFCFs for

the parallel and perpendicular polarization configurations are defined by

$$\langle \delta\omega(t)\delta\omega(0) \rangle_{\text{para}} = \sum_i P_i^{\text{XXXX}}(t)\delta\omega_i(t)\delta\omega_i(0) \quad (5a)$$

and

$$\langle \delta\omega(t)\delta\omega(0) \rangle_{\text{perp}} = \sum_i P_i^{\text{XXYY}}(t)\delta\omega_i(t)\delta\omega_i(0). \quad (5b)$$

$P_i^{\alpha\alpha\beta\beta}(t)$ is a time-dependent weighting factor given by

$$P_i^{\alpha\alpha\beta\beta}(t) = \frac{(\hat{\epsilon}_\alpha \cdot \hat{\mu}_i(t))^2 (\hat{\epsilon}_\beta \cdot \hat{\mu}_i(0))^2}{\sum_j (\hat{\epsilon}_\alpha \cdot \hat{\mu}_j(t))^2 (\hat{\epsilon}_\beta \cdot \hat{\mu}_j(0))^2}, \quad (5c)$$

where $\hat{\epsilon}_\alpha$ is the unit vector for the α -polarized electric field, and $\hat{\mu}_i(t)$ is the unit vector for molecule i 's transition dipole moment at time t . The denominator in (5c) is the normalization factor introduced such that $\sum_i P_i^{\alpha\alpha\beta\beta}(t) = 1$. The physical meaning of PW-FFCFs given in Eq. (5) can be understood in the following manner. If the dynamics of interest occur on a much longer timescale than the free-induction decay (FID), we may assume the first pair of field interactions is simultaneous, along with the final pair. The reorientation and spectral diffusion are observed here on a much longer time scale (Fig. 1) than the FID, which is almost complete within 1 ps. Under this short-time approximation, the weighting factor in (5c) gives the fraction of the i th molecule's contribution to the overall signal taken with each polarization configuration. The molecule interacts twice with the β -polarized incident E -field at $t = 0$ and then interacts with, and emits, an α -polarized E -field at time $t > 0$. Molecules with different orientations have different contributions to the observed signal, and the FFCFs weighted with these factors (5c) are the PW-FFCFs given in (5a) and (5b).

As a simple model calculation, we calculated the PW-FFCF observables for an ensemble of transition dipole moments experiencing orientational relaxation, with orientational diffusion constant, D , in a static electric field. We assume the frequency fluctuation $\delta\omega(t)$ is given by $\delta\vec{\mu} \cdot \vec{E}$, with the initial ensemble of transition dipole directions random relative to the electric field direction. The molecules (transition dipole directions) undergo orientational diffusion, and the observables are obtained from the ensemble averages over all initial dipole directions relative to the electric field and then an average over all electric field direction in the lab frame (frame relative to the laser beam polarizations). Thus, the frequency is determined by the time dependent Stark effect, with the time dependence caused by the orientational relaxation.

The Stark effect has been successfully used to describe inhomogeneous broadening and spectral diffusion for a variety of vibrational probes and environments.^{34,36-38} Mappings of the frequencies of hydrogen bonded hydroxyl oscillators to the local electric field as surrogates for the H-bond interactions have also proven useful in MD simulations of IR observables in solvents such as bulk water and ionic liquids.^{29,31,39,40} Compared to the solute's orientational motions, ionic liquids exhibit very slow global reorganization. The slow global structural randomization can result in a component of the electric field that evolves slowly compared to the vibrational

probe molecules' orientational relaxation. There are, however, components of the structural evolution that are much faster.^{27-29,41-44}

The full details of the calculations are given in the supplementary material.²⁶ The normalized PW-FFCFs, for the model of a transition dipole experiencing orientational diffusion around a fixed E -field, have analytical forms given by

$$\langle \delta\omega(t)\delta\omega(0) \rangle_{\text{para, norm}} = \frac{3}{25} \left[\frac{11C_1(t) + 4C_3(t)}{1 + 0.8C_2(t)} \right] \quad (6a)$$

and

$$\langle \delta\omega(t)\delta\omega(0) \rangle_{\text{perp, norm}} = \frac{3}{25} \left[\frac{7C_1(t) - 2C_3(t)}{1 - 0.4C_2(t)} \right]. \quad (6b)$$

Here $C_l(t) = \langle P_l(\hat{\mu}(0) \cdot \hat{\mu}(t)) \rangle$, with P_l the l th order Legendre polynomial. For orientational diffusion, $C_l(t) = \exp(-l(l+1)Dt)$. The PW-FFCFs in (6) are normalized to unity at $t = 0$. Within the context of the model, the isotropic, normalized FFCF without polarization-weighting was also calculated and found to be

$$\langle \delta\omega(t)\delta\omega(0) \rangle_{\text{norm}} = C_1(t). \quad (7)$$

This is the PW-FFCF which would result with magic angle polarized excitation beams, or equivalently for the isotropic combination $\langle \text{XXXX} \rangle + 2\langle \text{XXYY} \rangle$ signal, using the Stark model (see supplementary material).²⁶

The PW-FFCFs, the isotropic FFCF calculated with the model, and the orientational correlation function ($C_2(t)$, corresponding to the normalized pump-probe anisotropy) are plotted with respect to $D \times t$ in Fig. 2. The calculated PW-FFCFs for parallel and perpendicular polarization configurations are clearly distinguishable. As was observed experimentally (Fig. 1), the PW-FFCF for perpendicular polarization decays more rapidly than for parallel polarization. In these model calculations, the isotropic FFCF decays as a single exponential, and its decay time constant is exactly a

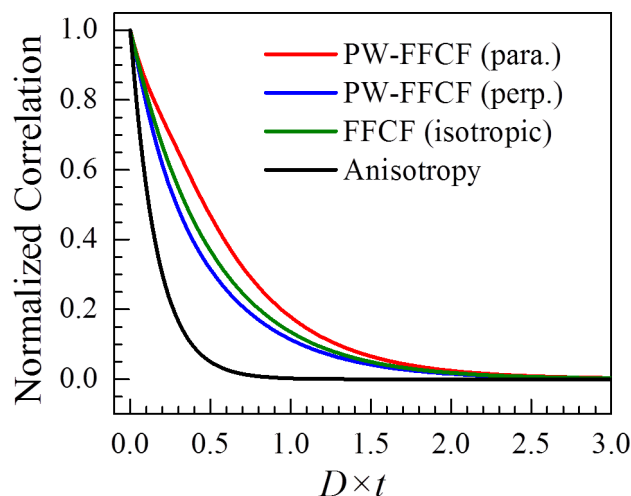


FIG. 2. Normalized frequency-frequency correlation functions calculated with the first order Stark model in the PW-FFCF formalism are plotted as functions of $D \times t$, with D the rotational diffusion constant. The normalized orientational anisotropy decay, $C_2(t)$, is shown for comparison and decays considerably more quickly than the FFCF curves as predicted.

factor of three longer than the anisotropy decay time constant. The perpendicular and parallel decays, which are somewhat faster and slower than the isotropic decay, respectively, are not exponential. Their shapes are determined by Eqs. (6a) and (6b). Although each $C_i(t)$ is an exponential, the combinations of the different exponential decays in Eq. (6) do not result in an exponential decay. However, if the curves are fit to single exponentials for comparison to the anisotropy decay, the perpendicular decay is a factor of 2.6 times slower than the anisotropy decay and the parallel decay is a factor of 3.7 times slower. These calculations strongly support our hypothesis that RISD is a significant spectral diffusion mechanism for the O–D stretch of methanol- d_4 in HmimPF₆.

The $\langle XYXY \rangle$ polarization configuration should be very useful in indicating whether reorientation-induced spectral diffusion contributes to the observed CLS decay; it shows a large difference from either the parallel or perpendicular polarization-selective CLS (Fig. 1). The PW-FFCF formulation (Eq. (5)) is clearly applicable to the parallel and perpendicular polarization configurations, where all the transition dipole moments emit signals in-phase with one another. However, in the polarization grating configuration, reorientation causes some of the dipoles to emit out-of-phase signals. The field-dipole dot products in (5c) no longer appear as squared terms at times zero and t and may be negative. Therefore, the weighting factor (5c), if constructed for the polarization grating configuration $\langle XYXY \rangle$, can no longer refer to a true probability distribution and the connection to an ensemble average is lost. However, the 2D IR line shape for $\langle XYXY \rangle$ is dependent on the line shapes in parallel and perpendicular polarization configurations and can be calculated as their difference (see supplementary material, Fig. S3).²⁶ The calculated CLS for $\langle XYXY \rangle$ (Fig. S4²⁶) exhibits a significantly slower decay than the parallel and perpendicular CLSs, which is again in agreement with the experimental data shown in Fig. 1.

V. SPECTRAL DIFFUSION THROUGH STRUCTURAL FLUCTUATIONS

Though the ordering of parallel and perpendicular PW-FFCFs decay rates is successfully reproduced by the model, the decay rates of PW-FFCFs with respect to the orientational correlation function are not in agreement with experiments. While the model calculations indicate that PW-FFCFs decay roughly 3 times more slowly than the orientational correlation function, the experimental CLS data for parallel and perpendicular polarization configurations decay much faster than would occur through RISD alone (Figs. 1(c) and 1(d)). This difference almost certainly originates from the contribution of structural spectral diffusion (SSD), which is not included in the model calculations. A liquid's structure will fully randomize on some timescale. Therefore, any local environment will eventually sample every possible configuration. Structural spectral diffusion can occur through fluctuating interactions that are not vectors, e.g., density fluctuations,⁴⁵ or through fluctuations that are fast compared to the orientational relaxation of the transition dipole. The vibrational probes are located in the ionic regions of the room temperature

ionic liquid (generally hydrogen bonded to anions⁴⁶). The ionic regions undergo structural fluctuations that are fast compared to the complete global structural randomization.^{28,42} If the vibrational probe reorientation is much slower than the structural fluctuations that sample all configurations that give rise to the inhomogeneously broadened absorption line,⁴⁵ then all spectral diffusion will be due to structural spectral diffusion. However, if some structural fluctuations are fast compared to the probes orientational relaxation and some are slow, then the total spectral diffusion can be a mix of structural spectral diffusion and reorientation induced spectral diffusion. The PW-FFCF technique can be augmented to model structural spectral diffusion as a combination of electric field amplitude and direction fluctuations on all time scales. When fast structural fluctuations are taken into account in the first-order Stark model discussed above, the spectral diffusion rates will be significantly accelerated. An extension of the theory presented here to include structural spectral diffusion is under development.

The relative rates of reorientation-induced spectral diffusion and structural spectral diffusion determine whether RISD is observed in the polarization-selective CLS or FFCF. Figure 3 shows CLS decays obtained on the O–D stretch of dilute HOD, singly deuterated water, in bulk H₂O with $\langle XXXX \rangle$, $\langle XXYX \rangle$, and $\langle XYXY \rangle$ polarization configurations. The data are identical within experimental error and can be simultaneously fit with a biexponential decay curve. Only the $\langle XYXY \rangle$ CLS data may be analyzed beyond $T_w = 2$ ps because isotropic heating artifacts^{2,47} are not detected with this polarization configuration. We obtain a FFCF consistent with that previously reported for this system.¹⁸ Representative 2D IR spectra at an intermediate waiting time are shown in the supplementary material (Fig. S5);²⁶ the 2D line shapes are virtually the same for the different polarization configurations. The correlation times of fits to the individual $\langle XXXX \rangle$, $\langle XXYX \rangle$, and $\langle XYXY \rangle$ CLS decays are in good agreement with the global fit to all three data sets (see supplementary material, Table SI).²⁶

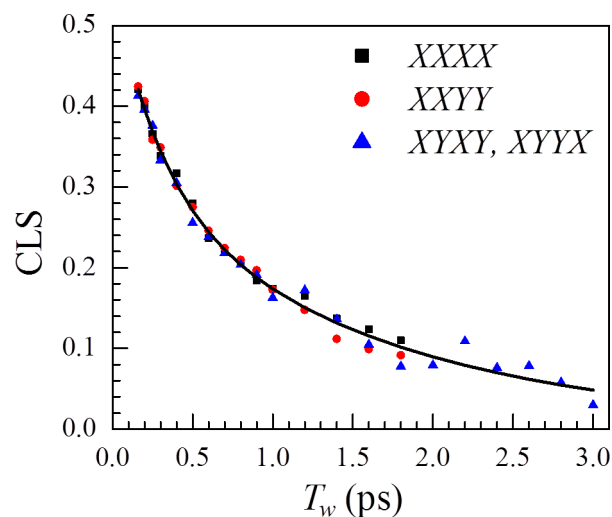


FIG. 3. Polarization-selective CLS decay of bulk water (4% HOD in H₂O) obtained with the polarization configurations $\langle XXXX \rangle$, $\langle XXYX \rangle$, and $\langle XYXY \rangle$. The data (points) taken with the three configurations are identical within experimental error. The solid line is a simultaneous biexponential fit to all three data sets, giving time constants 0.30 ± 0.07 ps and 1.6 ± 0.2 ps.

The majority (~80%) of the sampling of the inhomogeneous spectrum of the O–D stretch of HOD in water (see Figure S1 for spectrum) occurs on a time scale of <0.4 ps.¹⁸ The slowest component of the spectral diffusion is 1.7 ps.¹⁸ The orientational relaxation time measured by IR pump-probe experiments ($C_2(t)$) of HOD in water is 2.6 ps.^{2,18} The reorientation-induced contribution to the total spectral diffusion will occur on a time scale approximately a factor of three slower than the measured orientational relaxation time. Therefore, it is anticipated and observed that the RISD contribution is too slow to be detected in these 2D IR experiments.

Although the polarization-selective 2D IR spectra of water display no measurable RISD contribution, it is well known that the longer-timescale spectral diffusion of hydrogen bonded hydroxyl oscillators in water is caused predominantly by hydrogen bond rearrangement, which necessarily involves large angle hydroxyl orientational jumps.^{39,40,48,49} It is therefore expected that hydroxyl reorientation rates will be correlated with frequency fluctuations. Temperature-dependent studies have found that both the spectral and orientational diffusion rates of water hydroxyls scale with temperature in an approximately Arrhenius manner with similar barrier heights, suggesting they are activated by the same hydrogen bond rearrangement processes.^{48,49} Detailed 2D IR anisotropy experiments conducted by Ramasesha *et al.* have further shown that reorientation in water, in particular the ultrafast inertial orientational motion, can vary depending on the initial and final hydrogen bond strengths.²¹

However, there is a key difference between the correlation of orientational and spectral fluctuations that is well-established for water, and the strong vector dependence of the frequency fluctuation on probe orientation observed in the present work for methanol in the RTIL HmimPF₆. Methanol reorientation in the ionic liquid occurs without complete randomization of the liquid structure. A component of the structure that contributes to the overall inhomogeneous broadening of the absorption line shape can therefore be considered static on methanol orientational timescales. The fluctuation of the frequency, and therefore spectral diffusion, is a result of the time evolution of the probe's interaction with this static structural component through the transition dipole's angular motions, not through the structure itself changing. In HmimPF₆, reorientation of the methanol does not change the structural component of the system that contributes to the inhomogeneous broadening and that is static on the methanol orientational relaxation time scale. Only the coupling of the methanol to the vector interaction with the static structure changes with reorientation. The long lived structural component does not change with methanol reorientation, only the way methanol senses the long lived structure changes.

The situation in the methanol/RTIL system is very different from bulk water. No component of the structure in bulk water is static on the time scale of reorientation because reorientation is a major component of the structural reorganization mechanism.^{21,39,40,48,49} The hydroxyl (O–D stretch of HOD) will have different interactions with its environment through its own angular fluctuations. However, the structure is simultaneously evolving fast enough through this angular mo-

tion and the structural changes, including reorientation of other water molecules, that structural spectral diffusion determines the overall FFCF decay.

VI. CONCLUDING REMARKS

We have shown that different polarization configurations in 2D IR vibrational echo experiments can result in distinct measurements of spectral diffusion dynamics and therefore different frequency-frequency correlation functions. The differences with polarization are the result of reorientation-induced spectral diffusion, and we have presented a theoretical description of RISD. We have shown that RISD and structural spectral diffusion can be distinguished experimentally (Figs. 1 and 3) using polarization-selective 2D IR spectroscopy in conjunction with polarization-selective pump-probe experiments. The experimentally observed polarization-dependence of the time dependent two-dimensional band shapes results from the interesting properties of the ionic liquid structure; components of the global structure evolve very slowly, but the solute molecules can reorient relatively rapidly. If the angular motions of probe molecules are very slow relative to the complete structural evolution of the medium,^{11,34,45} the RISD contribution to spectral diffusion will be negligible and spectral diffusion will be caused entirely by structural fluctuations.

The polarization-selective 2D IR spectral diffusion measurements can provide new details of the coupling between angular coordinates and the intermolecular interactions that lead to inhomogeneous broadening and spectral diffusion in a wide variety of experimental systems. Such coupling can be important for solvation in complex materials (such as ionic liquids) and reactions in biological systems. Theory and model calculations presented here demonstrate that the differences between polarization-selective experimental CLS decays can be understood as the result of differently weighted ensembles of rotating probe molecules. A more complete model which incorporates RISD, SSD, and the effects of restricted orientational motion (wobbling-in-a-cone) on the CLS observable is under development.

ACKNOWLEDGMENTS

This work was funded by the Division of Chemical Sciences, Geosciences, and Biosciences, Office of Basic Energy Sciences of the U.S. Department of Energy through Grant No. DE-FG03-84ER13251 (P.L.K., C.H.G., and M.D.F.) and the Air Force Office of Scientific Research Grant No. FA9550-12-1-0050 (J.N., A.T., and M.D.F.). P.L.K., J.N., and A.T. acknowledge support from Stanford Graduate Fellowships.

¹H.-S. Tan, I. R. Piletic, and M. D. Fayer, *J. Opt. Soc. Am. B* **22**(9), 2009–2017 (2005).

²Y. L. A. Rezus and H. J. Bakker, *J. Chem. Phys.* **123**(11), 114502 (2005).

³M. Cho, G. R. Fleming, and S. Mukamel, *J. Chem. Phys.* **98**(7), 5314–5326 (1993).

⁴S. Mukamel, *Principles of Nonlinear Optical Spectroscopy* (Oxford University Press, New York, 1995).

⁵P. Hamm and M. T. Zanni, *Concepts and Methods of 2D Infrared Spectroscopy* (Cambridge University Press, Cambridge, New York, 2011).

⁶O. Golonzka and A. Tokmakoff, *J. Chem. Phys.* **115**, 297–309 (2001).

- ⁷R. M. Hochstrasser, *Chem. Phys.* **266**(2–3), 273–284 (2001).
- ⁸M. Ji, M. Odellius, and K. J. Gaffney, *Science* **328**(5981), 1003–1005 (2010).
- ⁹M. T. Zanni, N.-H. Ge, Y. S. Kim, and R. M. Hochstrasser, *Proc. Natl. Acad. Sci. U.S.A.* **98**(20), 11265–11270 (2001).
- ¹⁰S. Woutersen and P. Hamm, *J. Phys. Chem. B* **104**(47), 11316–11320 (2000).
- ¹¹J. Nishida, A. Tamimi, H. Fei, S. Pullen, S. Ott, S. M. Cohen, and M. D. Fayer, *Proc. Natl. Acad. Sci. U.S.A.* **111**(52), 18442–18447 (2014).
- ¹²C. R. Baiz, D. Schach, and A. Tokmakoff, *Opt. Express* **22**(15), 18724–18735 (2014).
- ¹³A. Tokmakoff, *J. Chem. Phys.* **105**(1), 1–12 (1996).
- ¹⁴A. Tokmakoff and M. D. Fayer, *J. Chem. Phys.* **103**, 2810 (1995).
- ¹⁵S. Park, K. Kwak, and M. D. Fayer, *Laser Phys. Lett.* **4**, 704–718 (2007).
- ¹⁶K. Kwak, S. Park, I. J. Finkelstein, and M. D. Fayer, *J. Chem. Phys.* **127**, 124503 (2007).
- ¹⁷K. Kwak, D. E. Rosenfeld, and M. D. Fayer, *J. Chem. Phys.* **128**(20), 204505 (2008).
- ¹⁸S. Park, D. E. Moilanen, and M. D. Fayer, *J. Phys. Chem. B* **112**(17), 5279–5290 (2008).
- ¹⁹S. T. Roberts, J. J. Loparo, and A. Tokmakoff, *J. Chem. Phys.* **125**(8), 084502 (2006).
- ²⁰F. Perakis and P. Hamm, *J. Phys. Chem. B* **115**(18), 5289–5293 (2011).
- ²¹K. Ramasesha, S. T. Roberts, R. A. Nicodemus, A. Mandal, and A. Tokmakoff, *J. Chem. Phys.* **135**(5), 054509 (2011).
- ²²G. Stirnemann and D. Laage, *J. Phys. Chem. Lett.* **1**(10), 1511–1516 (2010).
- ²³C. A. Rivera, A. J. Souna, J. S. Bender, K. Manfred, and J. T. Fourkas, *J. Phys. Chem. B* **117**(49), 15875–15885 (2013).
- ²⁴J. Helbing, K. Nienhaus, G. U. Nienhaus, and P. Hamm, *J. Chem. Phys.* **122**(12), 124505 (2005).
- ²⁵E. E. Fenn, D. B. Wong, and M. D. Fayer, *J. Chem. Phys.* **134**, 054512 (2011).
- ²⁶See supplementary material at <http://dx.doi.org/10.1063/1.4920949> for additional experimental methods, details of the polarization-weighted FFCF model calculations, and 2D IR spectra and CLS fit results for the HOD in bulk water experiments.
- ²⁷D. B. Wong, C. H. Giammanco, E. E. Fenn, and M. D. Fayer, *J. Phys. Chem. B* **117**, 623–635 (2012).
- ²⁸P. L. Kramer, C. H. Giammanco, and M. D. Fayer, *J. Chem. Phys.* **142**(21), 212408 (2015).
- ²⁹Z. L. Terranova and S. A. Corcelli, *J. Phys. Chem. B* **118**(28), 8264–8272 (2014).
- ³⁰J. T. Fourkas, R. Trebino, and M. D. Fayer, *J. Chem. Phys.* **97**(1), 69–77 (1992).
- ³¹S. Corcelli and J. L. Skinner, *J. Phys. Chem. A* **109**, 6154–6165 (2005).
- ³²D. E. Moilanen, E. E. Fenn, Y. S. Lin, J. L. Skinner, B. Bagchi, and M. D. Fayer, *Proc. Natl. Acad. Sci. U.S.A.* **105**(14), 5295–5300 (2008).
- ³³J. J. Loparo, C. J. Fecko, J. D. Eaves, S. T. Roberts, and A. Tokmakoff, *Phys. Rev. B* **70**(18), 180201 (2004).
- ³⁴R. B. Williams, R. F. Loring, and M. D. Fayer, *J. Phys. Chem. B* **105**, 4068–4071 (2001).
- ³⁵G. U. Bublitz and S. G. Boxer, *Annu. Rev. Phys. Chem.* **48**(1), 213–242 (1997).
- ³⁶P. L. Geissler, *Annu. Rev. Phys. Chem.* **64**(1), 317–337 (2013).
- ³⁷S. Bagchi, S. G. Boxer, and M. D. Fayer, *J. Phys. Chem. B* **116**, 4034–4042 (2012).
- ³⁸S. D. Fried, S. Bagchi, and S. G. Boxer, *J. Am. Chem. Soc.* **135**(30), 11181–11192 (2013).
- ³⁹S. Corcelli, C. P. Lawrence, and J. L. Skinner, *J. Chem. Phys.* **120**, 8107–8117 (2004).
- ⁴⁰C. P. Lawrence and J. L. Skinner, *J. Chem. Phys.* **118**, 264–272 (2003).
- ⁴¹A. L. Sturlaugson, A. Y. Arima, H. E. Bailey, and M. D. Fayer, *J. Phys. Chem. B* **117**, 14775–14784 (2013).
- ⁴²A. L. Sturlaugson, K. S. Fruchey, and M. D. Fayer, *J. Phys. Chem. B* **116**, 1777–1787 (2012).
- ⁴³Z. Hu and C. J. Margulis, *Acc. Chem. Res.* **40**(11), 1097–1105 (2007).
- ⁴⁴E. W. Castner, C. J. Margulis, M. Maroncelli, and J. F. Wishart, *Annu. Rev. Phys. Chem.* **62**(1), 85–105 (2011).
- ⁴⁵K. P. Sokolowsky, H. E. Bailey, and M. D. Fayer, *J. Chem. Phys.* **141**(19), 194502 (2014).
- ⁴⁶L. Cammarata, S. G. Kazarian, P. A. Salter, and T. Welton, *Phys. Chem. Chem. Phys.* **3**, 5192–5200 (2001).
- ⁴⁷T. Steinel, J. B. Asbury, J. R. Zheng, and M. D. Fayer, *J. Phys. Chem. A* **108**(50), 10957–10964 (2004).
- ⁴⁸R. A. Nicodemus, K. Ramasesha, S. T. Roberts, and A. Tokmakoff, *J. Phys. Chem. Lett.* **1**(7), 1068–1072 (2010).
- ⁴⁹R. A. Nicodemus, S. A. Corcelli, J. L. Skinner, and A. Tokmakoff, *J. Phys. Chem. B* **115**(18), 5604–5616 (2011).